Main Manuscript for

Transcranial stimulation of alpha oscillations modulates brain state dynamics in sustained attention

Joshua A. Brown[1*], Kevin J. Clancy[1], Chaowen Chen[1,2], Yimeng Zeng[3], Shaozheng Qin[3], Mingzhou Ding[4], & Wen Li[1*]

[1] Department of Psychology, Florida State University, Tallahassee, FL

[2] Tallahassee Memorial Healthcare, Tallahassee, FL

[3] State Key Laboratory of Cognitive Neuroscience and Learning, Beijing Normal University, Beijing, China

[4]J Crayton Pruitt Family Department of Biomedical Engineering, University of Florida, Gainesville, FL

*Corresponding authors: Joshua A. Brown, Wen Li; **Email:** jabrown@psy.fsu.edu; wenli@psy.fsu.edu

Author Contributions: J.A.B. & W.L. designed the research; K.J.C., C.C., and W.L. performed the research; S.Q. and Y.Z. contributed unpublished analytic tools; J.A.B., K.J.C., S.Q., Y.Z., M.D., and W.L. analyzed the data; J.A.B., K.J.C., C.C., S.Q., M.D., and W.L. wrote the paper.

Competing Interest Statement: The authors declare no competing financial interests.

Classification: Biological Sciences – Neuroscience; Social Sciences – Psychological and Cognitive Sciences

Keywords: complex systems, dynamics, hidden states, non-invasive brain stimulation (NIBS); simultaneous fMRI-tACS

This PDF file includes:

Main Text

Figures 1 to 4

Abstract

The brain is a complex system from which cognition is thought to arise as an emergent behavior, but the mechanisms underlying such processes remain unclear. We approached this problem based on the recognition of the two primary organizational architectures of the brain—large-scale networks and oscillatory synchrony—and their fundamental importance in cognition. Here, we applied high-definition alpha-frequency transcranial alternating-current stimulation (HD *α*-tACS) in a sustained attention task during functional resonance imaging (fMRI) to causally elucidate organizing principles of these major architectures (particularly, the role of alpha oscillatory synchrony) in cognition. We demonstrated that *α*-tACS both increased electroencephalogram (EEG) alpha power and improved sustained attention, degrees of which were positively correlated. Using Hidden Markov Modeling (HMM) of fMRI timeseries, we further uncovered five functionally important brain states (defined by distinct activity patterns of large-scale networks) and revealed the regulation of their temporal dynamics by *α*-tACS such that a Task-Negative state (characterized by activation of the default mode network/DMN) and Distraction state (with activation of the ventral attention and visual networks) was suppressed. These findings confirm the role of alpha oscillations in sustained attention, and more importantly, they afford a complex systems account that sustained attention is underpinned by multiple transient, recurrent brain states, whose dynamical balances are regulated by alpha oscillations. The study also highlights the efficacy of non-invasive oscillatory neuromodulation in probing the operation of the complex brain system and encourages future clinical applications to improve neural system health and cognitive performance.

Significance Statement

The brain operates a well-organized complex system to support mental activities. Along with well-known fluctuations in attention, we uncovered that the brain undergoes dynamic vacillations of functional states that are organized through large-scale neural networks and regulated by neural oscillations. We showcased that during sustained attention over an extended period time, the brain maintains a tug-of-war between functional “on” and “off” states. Applying *α*-tACS, we further demonstrated that the brain self-organizes this complex system through alpha oscillations, regulating the balance of such dynamic states in the upkeeping of cognitive performance.

Introduction

The human brain is an advanced complex system, and two mechanisms—large-scale neural networks and long-range oscillatory neural synchrony—are thought to serve as the primary organizational architectures of this system (1-4). Important insights into this organization in the human brain have emerged from functional magnetic resonance imaging (fMRI) and electro/magnetoencephalography (EEG/MEG) research through the identification of reliable intrinsic connectivity networks (such as the default mode network/DMN) and robust canonical oscillations (such as the alpha oscillation). Importantly, growing fMRI and EEG/MEG evidence converges to support the inherent synergy between the two organizational architectures such that the integration of large-scale neural networks both mediates (5) and is mediated by synchronized oscillations over multiple frequency bands (2-4).

Characteristic of a complex system, the brain is highly dynamical. The past few years have witnessed a major advance in characterizing the spatiotemporal dynamics of the brain in general and the large-scale networks and long-range synchrony specifically (1, 6). Beyond conventional analyses that assume stationarity and provide static (time-averaged) depictions of neural networks and oscillations, this rapidly developing research has identified transient and non-stationary recurring patterns of organized activity in the brain (known as “brain states”), both at rest and during task performance, and demonstrated their relevance to cognition and neuropsychiatric disorders (7-14). The reliable observation of the brain’s dynamic states notwithstanding, mechanistic understanding of the cause and regulation of such dynamics is largely unclear.

Dynamic fluctuations are also ubiquitous in cognitive processing and behavioral performance (15). Cognition requires the cooperation among distributed networks and is thought to arise as an emergent behavior of the brain’s complex system (6, 16). Correlational observations have implicated the dynamic brain states in various cognitive processes (17, 18) such as working memory (12, 13) and memory replay (8). Sustained attention (also known as vigilant attention or tonic alertness) is particularly characterized by substantial fluctuations over time and involves a distributed network of brain areas (19). Moreover, the neural mechanism underlying sustained attention is thought to fluctuate intrinsically (20). Specifically,

engagement and lapses of sustained attention have been associated with the intrinsic dynamic rivalry of opposing neural networks—the central executive network (CEN; alternatively, the frontoparietal network) and the task-negative network (dominated by the default mode network/DMN) (14, 21-23). In addition, neural synchrony in the alpha frequency has been associated with sustained attention and tonic alertness (20, 21, 24-28), and accordingly, alpha-frequency transcranial alternating current stimulation (*α*-tACS) that augmented alpha power has also been shown to enhance sustained attention (29). The foregoing thus suggests that sustained attention would provide an ideal model for the study of dynamic brain states, which, conversely, will offer novel systems-level insights into the neural underpinning of this important cognitive process.

Here, we approached these problems by leveraging the inherent coupling of alpha oscillations and large-scale neural network activity and manipulating the former to perturb brain state dynamics. Particularly, brain state dynamics characterized by DMN activity fluctuations have been repeatedly associated with the presence of strong alpha oscillations in humans (8, 30, 31). This potential synergy between the DMN and alpha oscillations aligns with a solid body of conventional (static) studies linking these two processes (32-39). Recently, experimental manipulations using *α*-tACS have further established that augmenting alpha oscillations would enhance both DMN fMRI functional connectivity (40) and DMN alpha oscillations (based on EEG source-level analysis, including both power (31) and connectivity (40)). Notably, to date, such changes have only been measured offline, and aftereffects of tACS could stem from different processes, precluding a direct inference of the coupling between the DMN and alpha oscillations. Nonetheless, a new rodent study applied simultaneous fMRI and theta-frequency optogenetic modulation and demonstrated the direct effect of theta oscillations in driving dynamic brain states (41), lending credence to such cooperation in humans and compelling the adoption of online brain recordings with brain stimulation in humans to approach such problems.

Therefore, we recorded fMRI simultaneously with high-definition (HD) *α*-tACS and combined it with a concurrent sustained attention task (the continuous performance task/CPT; **Fig. 1A**). Besides the DMN, we also incorporated other major cognitive networks (CEN and salience network/SN) (13), in addition to the

visual network (VN), given the visual task. Using hidden Markov Modelling (HMM) of fMRI timeseries from hubs of these large-scale networks (42), we extracted brain states and characterized their temporal dynamics over the 20-minute task (supplemental **Fig. S1**). After confirming its effects on static brain networks and CPT performance as previously reported (29, 31, 40), we tested the hypothesis that *α*-tACS would modulate the dynamics of brain states (i.e., upregulating task-positive and downregulating task-negative states) in the service of sustained attention.

RESULTS

α-tACS target engagement validation

As reported in (40), participants were randomly assigned to receive 20-minute active or sham HD α-tACS targeting the primary cortical source of alpha oscillations—the occipitoparietal cortex. We confirmed α-tACS -related alpha modulation as evinced by significant increase in both posterior alpha power and long-range posterior-to-frontal (P→F) alpha connectivity (measured with Granger causal/GC connectivity) in the Active (vs. Sham) group. This change was specific to the alpha frequency and absent in other frequencies. A separate, independent experiment including an active control group receiving α-tACS at random frequencies (1-200 Hz) replicated these effects while ruling out general frequency-non-specific effects. More details are provided in (40).

Behavioral effects: α-tACS improved high-load CPT performance

During the (active or sham) stimulation, participants completed the 20-minute CPT consisting of two cognitive load levels (low load: a single letter; high load: five letters). Hit rate was submitted to a repeated measures analysis of variance (ANOVA) of Load (high/low) and Group (Active/Sham), which confirmed a load effect: hit rate was significantly higher in the low- than high-load condition, $F(1,35) = 62.54$, $p < .001$, $\eta_p^2 = .64$. Importantly, as we predicted, there was a Group (i.e., tACS) effect: $F(1,35) = 3.19$, $p = .042$ one-tailed, $\eta_p^2 = .08$. Notably, as illustrated in **Fig. 1B** Left, this group effect was present primarily in the high load condition ($t(33.22) = 1.79$, $p = .042$ one-tailed), presumably due to a ceiling effect in the low load condition ($t(19.75) = 1.07$, $p = .149$ one-tailed). Further linking this behavioral improvement to α-tACS, we

confirmed a positive correlation between alpha power increase (Post – Pre tACS) and overall or high-load hit rate (*r*/*r* = .36/.36, *p* = .039/.037; **Fig. 1B** Right).

We also examined CPT performance based on the variability (the coefficient of variance/CV) of reaction times (RT) throughout the task. A similar ANOVA confirmed the effect of Load, $F(1,35) = 73.16$, $p < .001$, $\eta_p^2 = .68$; RT was more variable in the high- vs. low-Load condition. Confirming the association between RT variability and sustained attention, higher CV of RT was associated with lower hit rate ($r = -.57$, $p < .001$). However, there were no Group or Load-by-Group effects on RT variability (*p*'s > .66).

fMRI effects

Conventional (static) network analysis

As introduced above, fMRI was recorded during the CPT concurrently with stimulation, and timeseries data was drawn from 15 *a priori* regions of interest (ROIs) encompassing the hubs of DMN, CEN, SN, and VN. For validation, we first confirmed previous findings of α-tACS enhancing resting-state static connectivity in the DMN (40). Static (conventional time-averaged) DMN connectivity in the low load condition, which closely approximated a resting state given its minimal cognitive demand, was augmented relative to the pre-tACS baseline in the Active (vs. Sham) group (**Fig. 1C** Lower Left). For comparison, exploratory analyses outside the DMN discovered no connectivity change, highlighting the selective association between the DMN and alpha oscillations. Additionally, in the high load condition (**Fig. 1C** Upper Right), which clearly departed from a resting state, the group effect was not clearly present. More details are provided in *SI Appendix*.

Hidden brain states in sustained attention

fMRI timeseries from the ROIs were further submitted to hidden Markov modeling (HMM) to identify dynamic brain states (7, 42). We tested HMMs across a range of one to thirty states. Based on free energy (combined with the "kneedle" method (31, 43)), the 8-state HMM was determined as the optimal model (Supplemental **Fig. S1**; see more details in *SI Appendix*). This solution accords with previous studies that converged on HMMs of 8–12 states (7, 11, 30, 42).

Five of the eight states exhibited moderate-to-strong activation/deactivation (hence denoted as "active" states) in the networks while the other three showed minimal activation/deactivation (i.e., "non-active" states; **Fig. 2**). Based on their specific activation patterns (**Fig. 2**) and combined with the probabilistic time course and transition paths (**Fig. 3**), the five active states were labeled as: 1) "Initiation" state for the clear activation of CEN nodes (and moderate activation of the SN nodes) and the reliable emergence at the onset of (but rarely during) the task blocks (**Fig. 3B**), representative of an alert, active engagement state often observed at the beginning of a task or block; 2) "Task Positive" state for clear activation of the CEN nodes (and moderate activation of the SN nodes) and deactivation of the DMN nodes, consistent with a prototypical task-positive state; 3) "Task Negative" state for the clear activation of the DMN nodes and deactivation of the CEN (barring moderate activation of the left dlPFC) and SN nodes, consistent with a prototypical resting/task-negative state; 4) "Switch" state for the clear activation of dACC (and moderate DMN activation) and deactivation of the CEN nodes, resembling a transition zone between the task-negative and task-positive states (also see transition paths below); and 5) "Distraction" state for the strong right V2 activation, moderate right insula activation, and moderate posterior parietal cortex/PPC activation, which, together, resembled activation of the right-hemisphere dominant ventral attention network (44). Combined with the DMN deactivation, this state was thus characterized as the Distraction state, potentially induced by visual distractors in the high-load condition (see more discussion below).

This activation-based characterization of the states is confirmed by the state transition paths (**Fig. 3C&D**). Particularly, the Switch state appeared to be the transition hub among the active states, serving as the primary transition target for Task Negative state and Distraction state (transition probability = 54%/39%, respectively). While Task Positive state primarily transitioned to Distraction state (reflective of attention deterioration; transitional probability = 41%), its secondary transition target was Switch state (transitional probability = 28%). For outgoing transitions, Switch state transitioned primarily to Task Positive state and Task Negative state (transition probability = 35%/32%, respectively). Finally, the Initiation state exhibited low incoming transition probabilities, akin to its dominance at the beginning of each block. To further qualify and quantify these state transitions, we performed graph theoretical analysis of the transitional probabilities across participants (**Fig. 3D**). The degree centrality index for each state was computed for each subject

and submitted to an ANOVA, which showed a significant effect of state ($F(1,27) = 7.28$, $p < 0.001$, $\eta_p^2 = .20$). Akin to its rather exclusive presence at the beginning of each block, the Initiation state had the lowest degree centrality among all states (FDR *p*'s <0.045). In addition, the Switch state had numerically the highest degree centrality, which was statistically significantly higher than that of the Task Negative state (FDR $p = 0.025$).

Temporal dynamics of hidden brain states

We quantified the temporal dynamics of the five active states using two key metrics: fractional occupancy (FO; the percentage of the entire timeseries visited by a state, reflective of the prevalence of that state) and mean lifetime (ML; the average duration of a state visit, reflective of general durability). We then submitted these metrics for each state to separate ANOVAs (Load by Group) to examine the effect of *α*-tACS on these brain states.

Cognitive load modulated state dynamics

The manipulation of cognitive load significantly affected the FO and ML of the Task Negative state: high (vs. low) load reduced both the FO and ML of this state, $F(1,27) = 15.88$, $p < .001$ and $F(1,27) = 13.24$, $p = .001$, respectively (**Fig. 4A&B**). Cognitive load also affected the FO (albeit not ML) of the Task Positive state: FO was higher in the low (vs. high) load, $F(1,27) = 4.61$, $p = .041$. Other states did not exhibit effects of cognitive load (*p*'s > .26). Therefore, high cognitive load appeared to disrupt the Task Negative state by reducing its overall prevalence and durability and weaken the Task Positive state by reducing its overall prevalence.

α-tACS modulated state dynamics

The ANOVAs also revealed Group effects on state dynamics. In the Task Negative state, we observed a simple effect of Group on both FO and ML, $F(1,27) = 4.37$, $p = .047$ and $F(1,27) = 7.36$, $p = .012$, respectively, reflecting reduced FO and ML in the Active (vs. Sham) group (**Fig. 4A&B**). Furthermore, in the Distraction state, we observed an interaction between Group and Load on both FO and ML, $F(1,27) = 4.66$, $p = .040$ and $F(1,27) = 4.98$, $p = .034$, respectively. Specifically, as illustrated in **Fig. 4,** high load

increased the FO of the Distraction state in the Sham group ($t(14) = 2.10$, $p = .055$), but not in the Active group ($p = .348$). Similarly, ML of the Distraction state was lower for the Active (vs. Sham) group in the high load, $t(26) = 2.10$, $p = .003$, but equivalent for the groups in the low load ($p = .348$). These results suggest that tACS strengthened resistance to distractors in the high load condition. Other states did not exhibit any effects of Group either independently (p's > .09) or interactively with Load (p's > .19). Therefore, *α*-tACS suppressed Task Negative and Distraction states, especially at high cognitive load.

DISCUSSION

Combining HD *α*-tACS, simultaneous fMRI, and a sustained attention task (at low and high load) and applying HMM of fMRI timeseries in major large-scale networks, we uncovered a set of dynamical, functionally relevant brain states and revealed their responses to cognitive load and alpha modulation. Specifically, we delineated the temporal dynamics of Task Positive state, Task Negative state, and Distraction state, known to facilitate and interfere with sustained attention, respectively, providing mechanistic insights into this important cognitive process and its characteristic fluctuations. Critically, transcranial upregulation of alpha oscillations via *α*-tACS resulted in the suppression of the interfering states (i.e., Task Negative and Distraction states) and improvement in task performance, especially at high load, highlighting the role of alpha oscillations in regulating dynamics of neural networks and sustained attention. These findings provide causal insights into the operation of the brain's complex system while shedding light on systems-level mechanisms underlying cognition. Finally, that *α*-tACS selectively modulated two of the dynamic states highlights its dependence on and/or selectivity of ongoing brain states, bearing relevance to future closed-loop applications to optimize tACS.

Our *α*-tACS manipulation led to significant augmentation in alpha oscillations (both alpha power and long-range connectivity; as detailed in (40)). Here, we further demonstrated that it also increased hit rate in the sustained attention task (especially at high load), replicating a prior *α*-tACS study using a comparable task (29). Moreover, the degree of alpha augmentation positively predicted hit rates, directly linking *α*-tACS and the behavioral improvement. These findings add to the growing evidence for the active role of alpha oscillations in cognition (vs. the traditional view of cognitive disengagement or "idling"), particularly for

sustained attention and tonic alertness (20, 21, 24-28). Our conventional (static) functional connectivity analysis also revealed that *α*-tACS strengthened connectivity within (but not outside) the DMN, albeit only in the low load condition that closely approximated a resting state with its minimal cognitive demand. This online effect of *α*-tACS corroborates previously reported offline (Post – Pre) resting-state connectivity increase in the DMN (40), ruling out rebound effects for the offline finding and highlighting a direct, selective, and enduring effect of *α*-tACS on intrinsic DMN connectivity.

Our HMM analysis further identified five functionally relevant brain states during the sustained attention task and provided a cohesive depiction of their temporal dynamics. Critically, *α*-tACS modulated these dynamics, particularly in the high load condition, coinciding with the behavioral improvement at this load. It is worth noting the value and utility of such dynamic analysis, which was able to capture neural effects at high load that evaded the static analysis. Specifically, similar to an earlier study with interleaved low- and high-load blocks (13), we uncovered a state that emerged at the onset of every block, which was characterized by strong CEN and moderate SN activation, akin to the initiation (and transition) of the task (and load). In addition, attention engagement and lapses have been associated with the involvement of the CEN (aka, frontoparietal network) and the DMN, respectively (22), and indeed, we not only identified a Task Positive state (characterized by CEN activation and DMN deactivation) and a Task Negative state (characterized by DMN activation and CEN deactivation) but also revealed their responsiveness to cognitive load. Specifically, the load effect on the DMN-dominant (Task Negative) state (i.e., higher FO/ML at low than high load) corroborated the notion that the DMN is activated during rest and low-load tasks and de-activated during effortful tasks (45).

Furthermore, the brain vacillated between these two states via a Switch state. In keeping with this, the Switch state was more visited than other states, i.e., with greater FO than all other states (p's < .02) except for the Distraction state (p = .13; **Fig. 3C&D**). This frequent transition between Task-Positive and Negative states accords with constant fluctuations characteristic of sustained attention. It has been postulated that the vacillation between Task Positive and Task Negative states may reflect an adaptive process to prevent over-engagement of the CEN and over-disengagement of the DMN, which could undermine performance

(22). Therefore, attention fluctuation (especially, over an extended period of sustained attention) may reflect the rhythmicity of attention that is cognitively beneficial (46). Conversely, the absence of such fluctuating (or even labile) states (the perpetuation of a certain state thereof) would cause neural avalanches, resulting in cognitive impairments and even neuropsychiatric disorders (4). For instance, entanglement between the DMN and SN (14, 47) and low neural variability in all four networks (48) in attentional disorders (e.g., attention deficit hyperactivity disorder) could reflect disruptions in the dynamical fluctuation of brain states, underpinning its attentional impairments. In keeping with that, we observed that while improving the CPT accuracy, *α*-tACS did not reduce variability (CV of RT) of the performance. Consistently, we observed no effect of *α*-tACS on the transition rate of the brain states (*p*'s >.10). That is, while altering the balance between functionally beneficial and detrimental states (as discussed below), *α*-tACS preserved neural fluctuation (or rhythmicity) throughout the task.

Finally, we observed a Distraction state that was particularly pronounced at high load (characterized by the presence of distractors) in the Sham group. Interestingly, the Task Positive state was likely to transition into this Distraction state, which further transitioned into the Switch state or defaulted into the Task Negative state (**Fig. 3C&D; Fig. 4**). This suggests that attention lapses could arise as the Task Positive state is hijacked by distracting input. Importantly, both the Task-Negative and Distraction states were suppressed by *α*-tACS (**Fig. 4**), in keeping with the behavioral improvement it induced. It is also worth noting that efficacy of *α*-tACS has been shown to be state-dependent (49), and a study examining its aftereffect on dynamic brain states indicated that it primarily affected a DMN-dominant state (31). Therefore, the current finding underscores this state-dependent quality of alpha stimulation and its close association with DMN functioning, and thus promotes the application of closed-loop *α*-tACS to fully capitalize upon its neuromodulatory capacity.

The static and dynamic effects of *α*-tACS together causally illuminate how the brain's complex system operates on its primary architectures—large-scale networks and neural synchrony. Specifically, we surmise that at rest, alpha oscillations upkeep intrinsic DMN integrity whereas during task, they regulate the dynamic balance ("on" and "off") of large-scale neural networks that are conducive or disruptive to task performance.

This notion resonates with increasing recognition of the multifaceted, sometimes paradoxical, functions of alpha oscillations (27, 50). The former (supporting intrinsic DMN functioning at rest) features alpha oscillations as a "long-range communicator" (27, 50). That is, as reported in (40), the strengthening of intrinsic DMN connectivity via *α*-tACS was mediated by frontal-posterior alpha synchrony (indexed by posterior-to-frontal alpha-frequency Granger causality) but not by local alpha activity (indexed by alpha power). In comparison, the latter (regulating brain state dynamics during task, particularly sustained attention) exemplifies local modulation by alpha oscillations as a "sensory inhibitor" (that suppresses distracting information and thus a Distraction state) and a "vigilance maintainer" (that fends off a Task Negative state) (27, 50). In keeping with this latter function, we observed that not only task performance but also the durability (i.e., ML) of Distraction state was predicted by posterior alpha power (r = -.42, p = .037; see *SI Appendix*). Moreover, the strong right V2 activation in the Distraction state aligns with the right-hemisphere lateralization of local alpha inhibition of the sensory cortex (51). Consistent with previous combined EEG-fMRI studies (52, 53), this transient activation of the right V2 in the Distraction state likely reflects evasion from alpha inhibition (i.e., failed sensory gating or filtering), resulting in increased response to distracting visual stimuli. Together, behavioral and neural (static and dynamic) effects *α*-tACS coalesce to highlight and harmonize the complex functions of alpha oscillations.

In summary, current findings provide new insights into the dynamical organization of the brain activity that underpins cognition. Specifically, it presents a complex system perspective of the mechanism underlying sustained attention: the engagement of a tug-of-war between Task Positive and Task Negative brain states (along with resulting frequent switching between them) and the interception of the Task Positive state by distractors. Critically, alpha oscillations play a modulatory role in such dynamics of brain states, effectively shifting the balance in the tug-of-war (favoring beneficial over detrimental states). Consequent to the fine tuning of brain state dynamics, sustained attention performance would improve.

Materials and Methods

Participants

Forty-one healthy volunteers (24 females, 20.8 ± 3.2 years of age) participated in the experiment as a part of a large study (40). Participants reported no history of neurological or psychiatric disorders, current use of psychotropic medications, and had normal or corrected-to-normal vision. Participants were randomly and blindly assigned to the Active group (*n* = 21) or the Sham group (*n* = 20). Two participants (Active *n* =2) terminated the experiment due to discomfort in the MRI scanner. fMRI data were collected during the CPT from twenty-nine participants, and one Sham participant was excluded from analysis due to excessive motion, resulting in 28 participants for fMRI analysis (Active *n* = 13, Sham *n* = 15). Two Active participants were excluded for behavioral recording errors and failure to follow instructions, respectively, resulting in 37 participants for behavioral analyses (Active *n* = 17, Sham *n* = 20). The two groups did not differ in age or gender (*p*'s > .5). Experimental protocol was approved by Florida State University's Institutional Review Board.

Experimental Design

Participants performed a sustained attention task for 20 mins while fMRI data was collected and tACS or sham stimulation was delivered (**Fig. 1A**). Eyes-open resting state EEG and fMRI data were collected before and after the task as reported in (40).

Continuous Performance Task (CPT)

The continuous performance task (CPT) has been widely used to study sustained attention (54, 55). In this study, the CPT task included two conditions, a low-load condition (a single letter at center of the screen) and a high-load condition (5 equidistant letters encircling a central fixation point; **Fig. 1A**), each presented in two blocks in alternating orders counterbalanced across participants and groups. Each block consisted of 300 trials, each lasting 1000 ms for a total of five minutes. Participants were instructed to press a button when the letter "X" appeared on screen, which occurred on 12.5% of the trials in each block.

tACS

Alpha-frequency stimulation was administered for the entire 20 minutes of the CPT. A ±2 mA sinusoidal current oscillating at 10 Hz was applied using an MR-compatible High-Definition (HD) tACS system in a 4 × 1 montage over midline occipitoparietal sites, which were selected to maximally target the

primary cortical source of alpha oscillations—occipitoparietal cortex. Sham stimulation was similarly applied, but the current was on for the first and last 30 seconds of the 20-minute task. Blindness of group assignment were confirmed through a systematical assessment. More details are provided in (40).

MRI Acquisition and Preprocessing

Gradient-echo T2-weighted echoplanar images were acquired on a 3T Siemens Prisma MRI scanner using a 64-channel head coil with axial acquisition. Imaging parameters and preprocessing protocols were the same as described in (40).

Regions of Interest (ROIs)

The three major cognitive neural networks—DMN, CEN, and SN—and the visual network (VN) were included. A total of 15 regions of interest (ROIs) representing hub regions of the four networks were included. Specifically, the DMN ROIs included midline (medioprefrontal cortex/mPFC, ventral and dorsal posterior cingulate cortex/vPCC & dPCC) and lateral (left and right angular gyrus/AG) hubs of the DMN; CEN ROIs included the left/right dorsolateral prefrontal cortex (dlPFC) and the left/right posterior parietal cortex (PPC); the SN ROIs included dorsal anterior cingulate cortex (dACC) and left/right anterior insula (AI); and the VN ROIs included V1 and left/right V2. The CEN SN, and frontal and lateral DMN ROIs were defined by the Willard Atlas (56). The PCC subdivisions were individually defined using the Brainnetome Atlas (57). The VN ROIs were defined by a probabilistic atlas of the visual cortex (58, 59).

Hidden Markov Modeling (HMM)

Preprocessed fMRI timeseries from the entire task were drawn from the ROIs and submitted to modeling via the HMM-MAR toolbox (https://github.com/OHBA-analysis/HMM-MAR). From our models generated with between 1 and 30 states, we determined that the 8-state model optimally represented the data. The model fit was indexed by the free energy, Akaike Information Criterion (AIC), Bayesian information criterion (BIC), and integrated complete likelihood (ICL) metrics. More details are provided in *SI Appendix*.

Graph theoretical analysis

Graph theoretical analysis was performed on transition probabilities of the five "active" states using the Brain Connectivity Toolbox (https://github.com/brainlife/BCT) and visualized in Gephi (60). To examine centrality of the five states, we calculated degree Z-score for each of the states in each participant and submitted the values to statistical analysis.

Statistical analysis

Target engagement of tACS (increased alpha power and P→F alpha connectivity) was validated in (40). We then confirmed the previously reported effect of tACS in improving sustained attention (29) using conducting repeated measures analyses of variance (ANOVAs) of Load (high/low) and Group (active/sham) on CPT accuracy and coefficient of variance (CV) of RT, respectively. For this confirmatory analysis, statistical significance was set at $p < .05$ one-tailed. Other than confirmatory analyses on the DMN connectivity (see *SI Appendix)*, we applied false discovery rate/FDR correction on tests for all other connections. For hypothesis testing (regarding the dynamics of brain states), we conducted similar ANOVAs (Load by Group) on the FO and ML on the identified states, respectively. Statistical significance was set at $p < .05$ two-tailed.

Acknowledgments

This research was supported by the National Institutes of Health grants (R21MH126479, R01MH132209, and R01NS129059 W.L.) and the FSU Chemical Senses Training (CTP) Grant Award T32DC000044 (K.C.) from the National Institutes of Health (NIH/NIDCD).

References

1. G. Deco, M. Corbetta, The dynamical balance of the brain at rest. *Neuroscientist* **17**, 107-123 (2011).
2. M. Shanahan, Metastable chimera states in community-structured oscillator networks. *Chaos* **20**, 013108 (2010).
3. F. Varela, J.-P. Lachaux, E. Rodriguez, J. Martinerie, The brainweb: Phase synchronization and large-scale integration. *Nature Reviews Neuroscience* **2**, 229-239 (2001).
4. G. Buzsaki, A System of Rhythms: From simple to complex dynamics. *Rhythms of the Brain*, 111-135 (2006).
5. M. Schneider *et al.*, A mechanism for inter-areal coherence through communication based on connectivity and oscillatory power. *Neuron* **109**, 4050-4067. e4012 (2021).
6. M. Breakspear, Dynamic models of large-scale brain activity. *Nature neuroscience* **20**, 340-352 (2017).
7. D. Vidaurre *et al.*, Discovering dynamic brain networks from big data in rest and task. *Neuroimage* **180**, 646-656 (2018).
8. C. Higgins *et al.*, Replay bursts in humans coincide with activation of the default mode and parietal alpha networks. *Neuron* **109**, 882-893. e887 (2021).
9. E. Damaraju *et al.*, Dynamic functional connectivity analysis reveals transient states of dysconnectivity in schizophrenia. *NeuroImage: Clinical* **5**, 298-308 (2014).
10. K. Supekar, W. Cai, R. Krishnadas, L. Palaniyappan, V. Menon, Dysregulated brain dynamics in a triple-network saliency model of schizophrenia and its relation to psychosis. *Biological psychiatry* **85**, 60-69 (2019).
11. J. N. v. d. Meer, M. Breakspear, L. J. Chang, S. Sonkusare, L. Cocchi, Movie viewing elicits rich and reliable brain state dynamics. *Nature communications* **11**, 5004 (2020).
12. U. Braun *et al.*, Brain network dynamics during working memory are modulated by dopamine and diminished in schizophrenia. *Nature communications* **12**, 3478 (2021).
13. J. Taghia *et al.*, Uncovering hidden brain state dynamics that regulate performance and decision-making during cognition. *Nature communications* **9**, 2505 (2018).
14. W. Cai *et al.*, Latent brain state dynamics distinguish behavioral variability, impaired decision-making, and inattention. *Molecular psychiatry* **26**, 4944-4957 (2021).
15. Timothy J. Buschman, S. Kastner, From Behavior to Neural Dynamics: An Integrated Theory of Attention. *Neuron* **88**, 127-144 (2015).
16. K. Friston, J. Kilner, L. Harrison, A free energy principle for the brain. *Journal of physiology-Paris* **100**, 70-87 (2006).
17. J. Gonzalez-Castillo, P. A. Bandettini, Task-based dynamic functional connectivity: Recent findings and open questions. *NeuroImage* **180**, 526-533 (2018).
18. V. Menon, Large-scale brain networks and psychopathology: a unifying triple network model. *Trends in cognitive sciences* **15**, 483-506 (2011).
19. R. Langner, S. B. Eickhoff, Sustaining attention to simple tasks: a meta-analytic review of the neural mechanisms of vigilant attention. *Psychological bulletin* **139**, 870 (2013).
20. R. F. Helfrich *et al.*, Neural Mechanisms of Sustained Attention Are Rhythmic. *Neuron* **99**, 854-865.e855 (2018).
21. M. S. Clayton, N. Yeung, R. C. Kadosh, The roles of cortical oscillations in sustained attention. *Trends in cognitive sciences* **19**, 188-195 (2015).
22. M. Esterman, D. Rothlein, Models of sustained attention. *Current opinion in psychology* **29**, 174-180 (2019).
23. F. C. Fortenbaugh, D. Rothlein, R. McGlinchey, J. DeGutis, M. Esterman, Tracking behavioral and neural fluctuations during sustained attention: A robust replication and extension. *Neuroimage* **171**, 148-164 (2018).
24. S. Makeig, M. Inlow, Lapse in alertness: coherence of fluctuations in performance and EEG spectrum. *Electroencephalography and clinical neurophysiology* **86**, 23-35 (1993).
25. C. Braboszcz, A. Delorme, Lost in thoughts: neural markers of low alertness during mind wandering. *Neuroimage* **54**, 3040-3047 (2011).

26. P. M. Dockree, S. P. Kelly, J. J. Foxe, R. B. Reilly, I. H. Robertson, Optimal sustained attention is linked to the spectral content of background EEG activity: Greater ongoing tonic alpha (~ 10 Hz) power supports successful phasic goal activation. *European Journal of Neuroscience* **25**, 900-907 (2007).
27. S. Sadaghiani, A. Kleinschmidt, Brain networks and α-oscillations: structural and functional foundations of cognitive control. *Trends in cognitive sciences* **20**, 805-817 (2016).
28. W. Klimesch, alpha-band oscillations, attention, and controlled access to stored information. *Trends Cogn Sci* **16**, 606-617 (2012).
29. M. S. Clayton, N. Yeung, R. Cohen Kadosh, Electrical stimulation of alpha oscillations stabilizes performance on visual attention tasks. *Journal of experimental psychology. General* **148**, 203-220 (2019).
30. D. Vidaurre *et al.*, Spontaneous cortical activity transiently organises into frequency specific phase-coupling networks. *Nature communications* **9**, 2987 (2018).
31. F. H. Kasten, C. S. Herrmann, The hidden brain-state dynamics of tACS aftereffects. *NeuroImage* **264**, 119713 (2022).
32. E. Tagliazucchi, F. von Wegner, A. Morzelewski, V. Brodbeck, H. Laufs, Dynamic BOLD functional connectivity in humans and its electrophysiological correlates. *Frontiers in human neuroscience* **6**, 339 (2012).
33. W. Tang *et al.*, Dynamic connectivity modulates local activity in the core regions of the default-mode network. *Proc Natl Acad Sci U S A* **114**, 9713-9718 (2017).
34. M. J. Brookes *et al.*, Investigating the electrophysiological basis of resting state networks using magnetoencephalography. *Proceedings of the National Academy of Sciences* **108**, 16783-16788 (2011).
35. J. Mo, Y. Liu, H. Huang, M. Ding, Coupling between visual alpha oscillations and default mode activity. *Neuroimage* **68**, 112-118 (2013).
36. G. G. Knyazev, J. Y. Slobodskoj-Plusnin, A. V. Bocharov, L. V. Pylkova, The default mode network and EEG alpha oscillations: an independent component analysis. *Brain Res* **1402**, 67-79 (2011).
37. K. Jann *et al.*, BOLD correlates of EEG alpha phase-locking and the fMRI default mode network. *Neuroimage* **45**, 903-916 (2009).
38. J. Samogin, Q. Liu, M. Marino, N. Wenderoth, D. Mantini, Shared and connection-specific intrinsic interactions in the default mode network. *Neuroimage* **200**, 474-481 (2019).
39. R. Scheeringa, K. M. Petersson, A. Kleinschmidt, O. Jensen, M. C. M. Bastiaansen, EEG alpha power modulation of fMRI resting-state connectivity. *Brain connectivity* **2**, 254-264 (2012).
40. K. J. Clancy *et al.*, Transcranial stimulation of alpha oscillations up-regulates the default mode network. *Proceedings of the National Academy of Sciences* **119**, e2110868119 (2022).
41. P. Salvan *et al.*, Frequency modulation of entorhinal cortex neuronal activity drives distinct frequency-dependent states of brain-wide dynamics. *Cell Reports* **37**, 109954 (2021).
42. D. Vidaurre, S. M. Smith, M. W. Woolrich, Brain network dynamics are hierarchically organized in time. *Proceedings of the National Academy of Sciences* **114**, 12827-12832 (2017).
43. V. Satopaa, J. Albrecht, D. Irwin, B. Raghavan (2011) Finding a" kneedle" in a haystack: Detecting knee points in system behavior. in *2011 31st international conference on distributed computing systems workshops* (IEEE), pp 166-171.
44. M. Corbetta, G. Patel, G. L. Shulman, The reorienting system of the human brain: from environment to theory of mind. *Neuron* **58**, 306-324 (2008).
45. M. E. Raichle, The brain's default mode network. *Annual review of neuroscience* **38**, 433-447 (2015).
46. I. C. Fiebelkorn, S. Kastner, A rhythmic theory of attention. *Trends in cognitive sciences* **23**, 87-101 (2019).
47. L. Sun *et al.*, Abnormal functional connectivity between the anterior cingulate and the default mode network in drug-naïve boys with attention deficit hyperactivity disorder. *Psychiatry Research: Neuroimaging* **201**, 120-127 (2012).
48. Z. Hu *et al.*, Disrupted signal variability of spontaneous neural activity in children with attention-deficit/hyperactivity disorder. *Biomedical Optics Express* **12**, 3037-3049 (2021).
49. S. Alagapan *et al.*, Modulation of Cortical Oscillations by Low-Frequency Direct Cortical Stimulation Is State-Dependent. *PLoS Biol* **14**, e1002424 (2016).

50. M. S. Clayton, N. Yeung, R. Cohen Kadosh, The many characters of visual alpha oscillations. *European Journal of Neuroscience* **48**, 2498-2508 (2018).
51. J. Jia, Y. Fan, H. Luo, Alpha-band phase modulates bottom-up feature processing. *Cerebral Cortex* **32**, 1260-1268 (2022).
52. R. Becker, M. Reinacher, F. Freyer, A. Villringer, P. Ritter, How ongoing neuronal oscillations account for evoked fMRI variability. *Journal of Neuroscience* **31**, 11016-11027 (2011).
53. S. D. Mayhew, D. Ostwald, C. Porcaro, A. P. Bagshaw, Spontaneous EEG alpha oscillation interacts with positive and negative BOLD responses in the visual–auditory cortices and default-mode network. *Neuroimage* **76**, 362-372 (2013).
54. H. E. Rosvold, A. F. Mirsky, I. Sarason, E. D. Bransome Jr, L. H. Beck, A continuous performance test of brain damage. *Journal of consulting psychology* **20**, 343 (1956).
55. J. Li *et al.*, Default mode and visual network activity in an attention task: Direct measurement with intracranial EEG. *Neuroimage* **201**, 116003 (2019).
56. A. Altmann, B. Ng, S. M. Landau, W. J. Jagust, M. D. Greicius, Regional brain hypometabolism is unrelated to regional amyloid plaque burden. *Brain* **138**, 3734-3746 (2015).
57. L. Fan *et al.*, The human brainnetome atlas: a new brain atlas based on connectional architecture. *Cerebral cortex* **26**, 3508-3526 (2016).
58. L. Wang, R. E. Mruczek, M. J. Arcaro, S. Kastner, Probabilistic maps of visual topography in human cortex. *Cerebral cortex* **25**, 3911-3931 (2015).
59. S. Yin *et al.*, Fear conditioning prompts sparser representations of conditioned threat in primary visual cortex. *Social Cognitive and Affective Neuroscience* **15**, 950-964 (2020).
60. M. Bastian, S. Heymann, M. Jacomy, Gephi: An Open Source Software for Exploring and Manipulating Networks. *Proceedings of the International AAAI Conference on Web and Social Media* (2009).

Figure Captions

Figure 1. Methods. A) Experimental Paradigm. Top: α-tACS or sham stimulation was delivered with simultaneous fMRI recordings while participants performed a sustained attention task. The task (Continuous Performance Task/CPT) consisted of four 5-minute blocks alternating between high and low load conditions (order of the conditions was counterbalanced across participants). Below: Example trials of the task. **B)** CPT performance. Left: The high load condition had lower hit rate than the low load condition in general, but α-tACS (vs. sham control) improved hit rate in the high load condition. Center red lines represent the mean values, with the pink and blue boxes representing the mean +/- 1.96 SEM and the mean +/- 1.5 SD, respectively. Right: alpha change (Post – Pre) predicted performance (hit rate) in both the high load (Top) and overall task (Bottom). Active and Sham groups are represented by filled and opened bars and dots, respectively. Dotted pink lines represent 95% confidence interval of least-squares regression line.* = $p < 0.05$; *** $p = < 0.001$. **C)** Conventional network analysis. Differential (Active – Sham) static functional connectivity (Fisher Z-transformed correlations)] matrix for the 15 *a priori* ROIs in low (Lower Left) and high (Upper Right) load conditions. Confirmatory analysis of default mode network (DMN) connectivity demonstrated strengthened connectivity in the DMN for the Active (vs. Sham) group, albeit in the low (but not high) load only. By contrast, significant group effects were absent outside the DMN, highlighting the selective association between the DMN and alpha oscillations. DMN includes mPFC (medial prefrontal cortex), vPCC (ventral posterior cingulate cortex), dPCC (dorsal posterior cingulate cortex), and l/r AG (left/right angular gyrus); CEN (central executive network) includes l/r dlPFC(left/right dorsolateral prefrontal cortex), and l/r PPC (left/right posterior parietal cortex); SN (salience network) includes dACC (dorsal anterior cingulate cortex) and l/r AI (left/right anterior insula); and VN (visual network) incudes V1 and l/r V2. . = $p < .05$, uncorrected; .. = $p < .01$, uncorrected; ** = $p < .01$, FDR corrected.

Figure 2. Dynamic brain states during the CPT. **A)** Average activation of each ROI (hub region) of the four networks within each state during the CPT. Positive and negative values indicate higher and lower average BOLD intensities within a given state relative to mean BOLD intensity for the entire CPT, reflecting relative activation and deactivation, respectively. Eight states were identified, including five states with clear

ROI activation/deactivation and three states with minimal ROI activation/deactivation. The five ("active") states were labeled according to their activation/deactivation patterns (as well as transition paths; detailed in **Fig. 3**). **B)** Normalized activation patterns of the five ("active") states. Radial plots (Top) and brain models (Bottom) illustrate normalized activation/deactivation levels, i.e., the percent change from baseline of each ROI relative to its maximal activation or deactivation across states. States are color-coded (and henceforth). Top row of brain models is lateral view, and bottom row is medial view. Spheres represent centroids of the anatomical masks of ROIs.

Figure 3. Temporal dynamics of the brain states. **A)** Time courses of all eight states for each participant (based on Viterbi decoding). The onset of each block is marked by a vertical dashed line. **B)** Consistency of state expression across participants for the five ("active") states. Values indicate the proportion of participants exhibiting the dominant state (based on Viterbi decoding) within a window of 10 TRs (11). Vertical dashed lines represent onset of task blocks. Horizontal dashed lines represent chance level, i.e., 1 of 8 states (12.5%) being predominantly expressed. **C)** Transition (to and from) probabilities (adjusted for the five active states) for each of the five states, averaged across all participants and task blocks. **D)** (Left) Graph of transition paths between states. Node size represents the fractional occupancy (FO; reflective of overall prevalence of a given state across the duration of the CPT) of each of the five states. Edge thickness represents the transition probabilities. The Switch state was the state with not only the highest FO but also strongest edges. The Task Negative ("Task –") state tended to transition to the Switch state while the Task Positive ("Task +") state primarily transitioned to the Distraction state, which then transitioned to the Switch or the Task Negative state. The weakest decile of transition probabilities is not shown. (Right) Centrality (Degree Z-score) of states in the transition graph at individual and group levels. As with edge thickness, the Initiation state had the lowest degree centrality while the the Switch state and, to some extent, the Distraction state had the highest degree centrality, reflective of their roles in mediating state transitions. Each dot represents an individual participant, and center red lines represent the mean values, with the grey box and the encompassing box representing the mean +/- 1.96 SEM and the mean +/- 1 SD, respectively.

Figure 4. Effects of α-tACS on temporal dynamics of the states. A) Fractional occupancy (FO) and **B)** Mean lifetime (ML) for the five "active" states of the Active (closed circles and boxes) and Sham (open circles and boxes) groups. Cognitive load reduced the FO and ML of the Task Negative ("Task –") state and the FO of the Task Positive ("Task +") state. Importantly, α-tACS reduced the FO and ML of the Task Negative state, regardless of load levels. Furthermore, interaction effects of Group and Load on FO and ML of the Distraction state indicate that α-tACS downregulated this state in the high load. Center red lines represent the mean values, with the grey box and the encompassing box representing the mean +/- 1.96 SEM and the mean +/- 1 SD, respectively. * $p < 0.05$; ** $p < 0.01$; † $p < 0.1$.

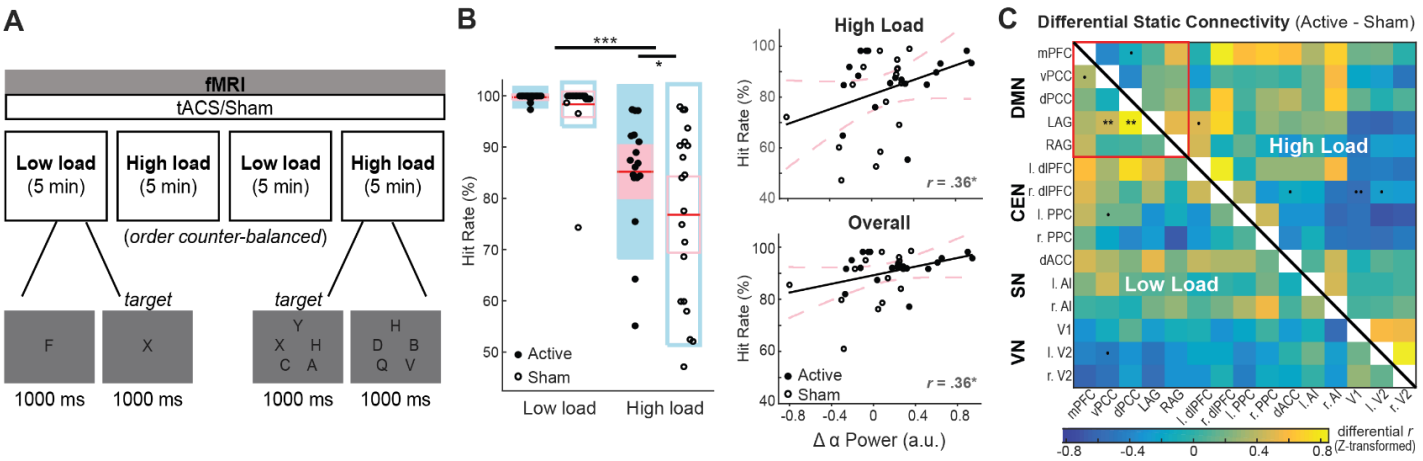

Figure 1. Methods. A) Experimental Paradigm. Top: α-tACS or sham stimulation was delivered with simultaneous fMRI recordings while participants performed a sustained attention task. The task (Continuous Performance Task/CPT) consisted of four 5-minute blocks alternating between high and low load conditions (order of the conditions was counterbalanced across participants). Below: Example trials of the task. **B)** CPT performance. Left: The high load condition had lower hit rate than the low load condition in general, but α-tACS (vs. sham control) improved hit rate in the high load condition. Center red lines represent the mean values, with the pink and blue boxes representing the mean +/- 1.96 SEM and the mean +/- 1.5 SD, respectively. Right: alpha change (Post – Pre) predicted performance (hit rate) in both the high load (Top) and overall task (Bottom). Active and Sham groups are represented by filled and opened bars and dots, respectively. Dotted pink lines represent 95% confidence interval of least-squares regression line.* = $p < 0.05$; *** $p = < 0.001$. **C)** Conventional network analysis. Differential (Active – Sham) static functional connectivity (Fisher Z-transformed correlations)] matrix for the 15 *a priori* ROIs in low (Lower Left) and high (Upper Right) load conditions. Confirmatory analysis of default mode network (DMN) connectivity demonstrated strengthened connectivity in the DMN for the Active (vs. Sham) group, albeit in the low (but not high) load only. By contrast, significant group effects were absent outside the DMN, highlighting the selective association between the DMN and alpha oscillations. DMN includes mPFC (medial prefrontal cortex), vPCC (ventral posterior cingulate cortex), dPCC (dorsal posterior cingulate cortex), and l/r AG (left/right angular gyrus); CEN (central executive network) includes l/r dlPFC(left/right dorsolateral prefrontal cortex), and l/r PPC (left/right posterior parietal cortex); SN (salience network) includes dACC (dorsal anterior cingulate cortex) and l/r AI (left/right anterior insula); and VN (visual network) incudes V1 and l/r V2. . = $p < .05$, uncorrected; .. = $p < .01$, uncorrected; ** = $p < .01$, FDR corrected.

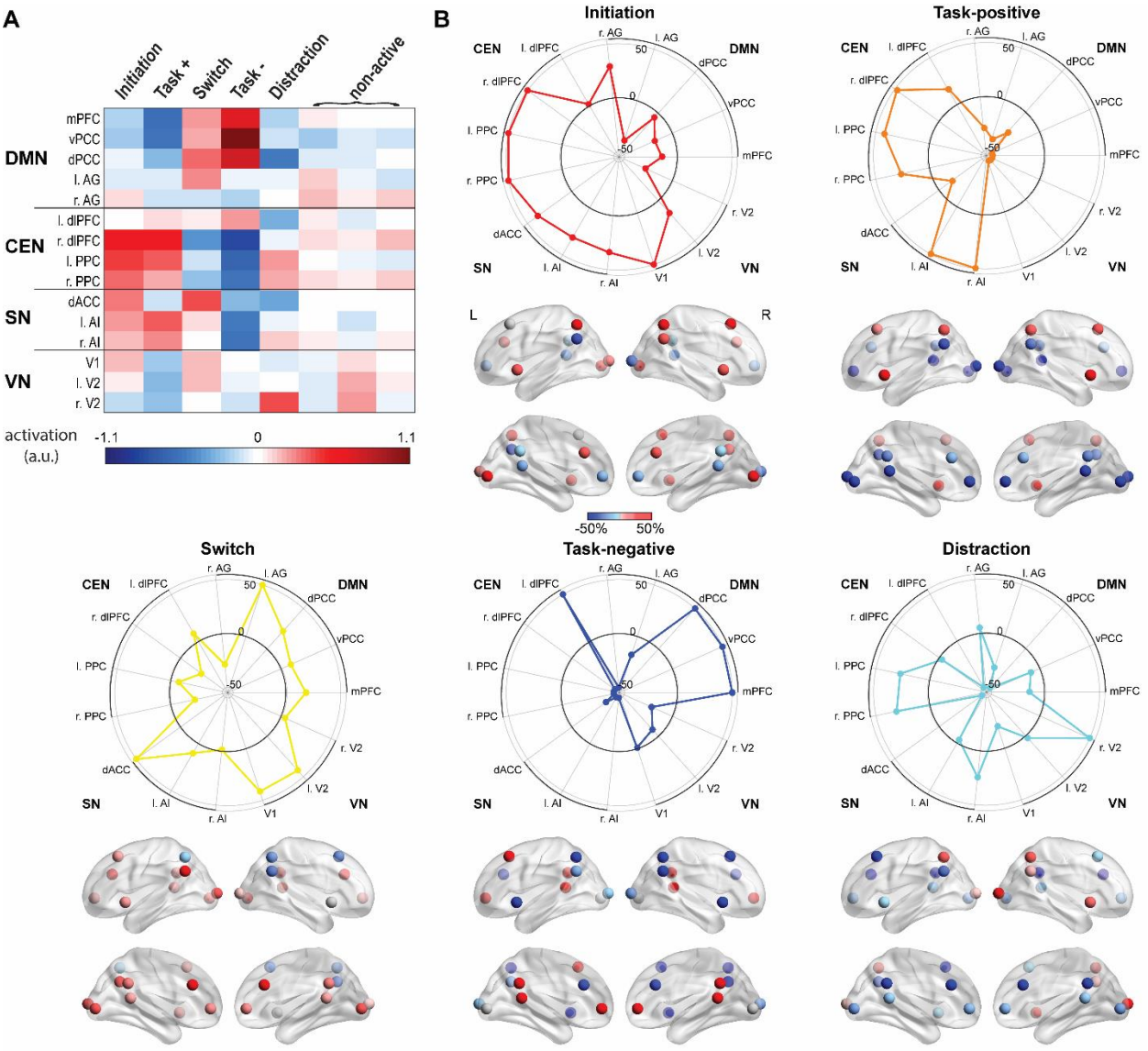

Figure 2. Dynamic brain states during the CPT. **A)** Average activation of each ROI (hub region) of the four networks within each state during the CPT. Positive and negative values indicate higher and lower average BOLD intensities within a given state relative to mean BOLD intensity for the entire CPT, reflecting relative activation and deactivation, respectively. Eight states were identified, including five states with clear ROI activation/deactivation and three states with minimal ROI activation/deactivation. The five ("active") states were labeled according to their activation/deactivation patterns (as well as transition paths; detailed in **Fig. 3**). **B)** Normalized activation patterns of the five ("active") states. Radial plots (Top) and brain models (Bottom) illustrate normalized activation/deactivation levels, i.e., the percent change from baseline of each ROI relative to its maximal activation or deactivation across states. States are color-coded (and henceforth).

Top row of brain models is lateral view, and bottom row is medial view. Spheres represent centroids of the anatomical masks of ROIs.

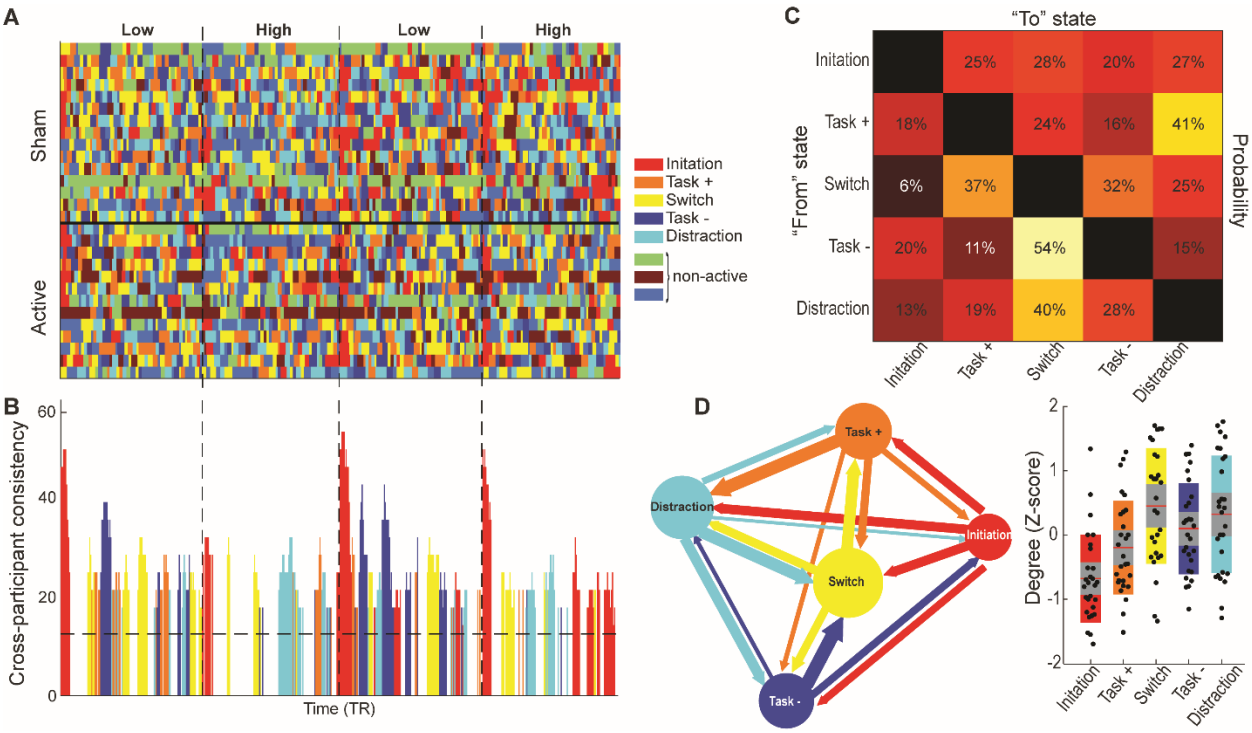

Figure 3. Temporal dynamics of the brain states. **A)** Time courses of all eight states for each participant (based on Viterbi decoding). The onset of each block is marked by a vertical dashed line. **B)** Consistency of state expression across participants for the five ("active") states. Values indicate the proportion of participants exhibiting the dominant state (based on Viterbi decoding) within a window of 10 TRs (11). Vertical dashed lines represent onset of task blocks. Horizontal dashed lines represent chance level, i.e., 1 of 8 states (12.5%) being predominantly expressed. **C)** Transition (to and from) probabilities (adjusted for the five active states) for each of the five states, averaged across all participants and task blocks. **D)** (Left) Graph of transition paths between states. Node size represents the fractional occupancy (FO; reflective of overall prevalence of a given state across the duration of the CPT) of each of the five states. Edge thickness represents the transition probabilities. The Switch state was the state with not only the highest FO but also strongest edges. The Task Negative ("Task –") state tended to transition to the Switch state while the Task Positive ("Task +") state primarily transitioned to the Distraction state, which then transitioned to the Switch

or the Task Negative state. The weakest decile of transition probabilities is not shown. (Right) Centrality (Degree Z-score) of states in the transition graph at individual and group levels. As with edge thickness, the Initiation state had the lowest degree centrality while the the Switch state and, to some extent, the Distraction state had the highest degree centrality, reflective of their roles in mediating state transitions. Each dot represents an individual participant, and center red lines represent the mean values, with the grey box and the encompassing box representing the mean +/- 1.96 SEM and the mean +/- 1 SD, respectively.

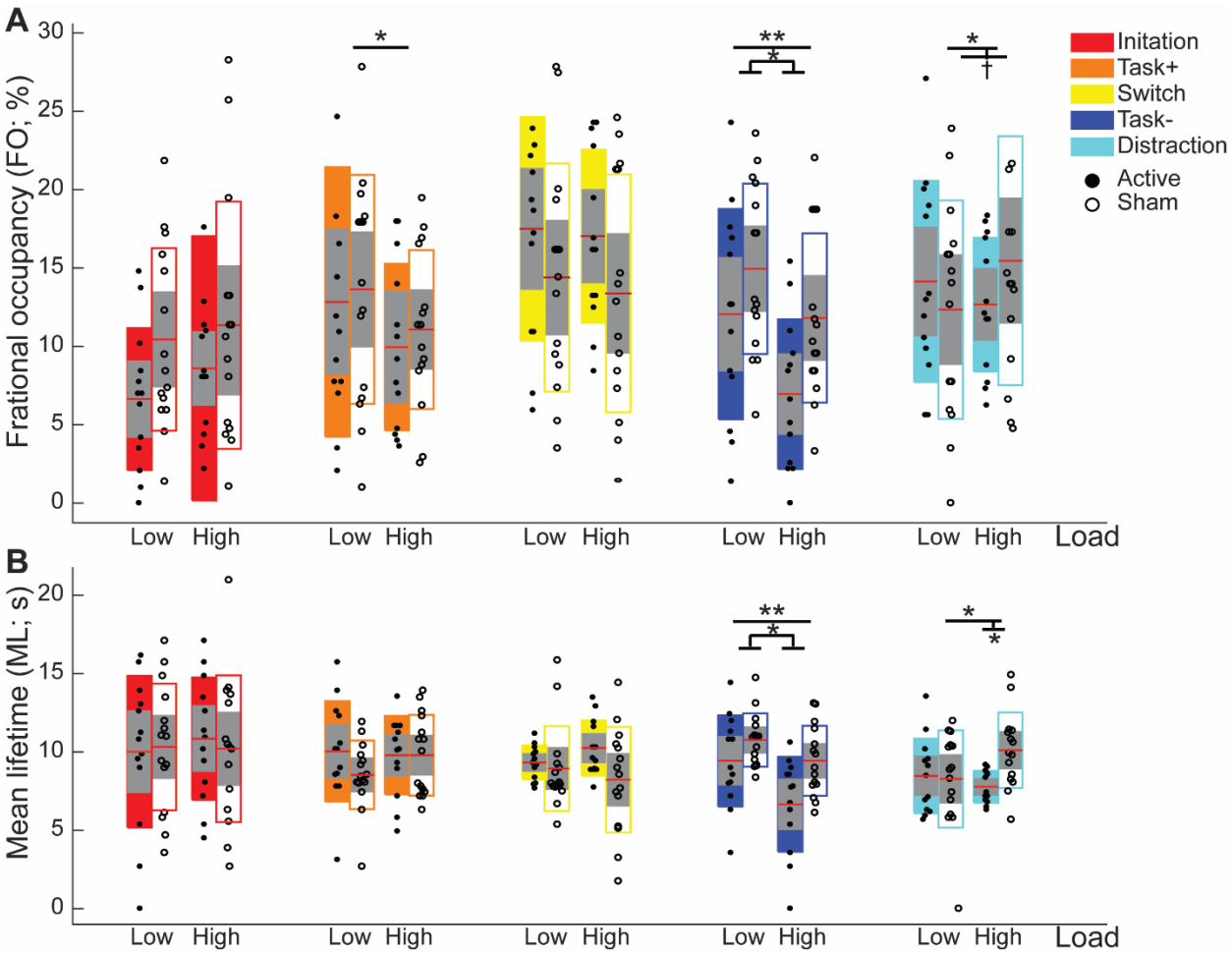

Figure 4. Effects of α-tACS on temporal dynamics of the states. A) Fractional occupancy (FO) and **B)** Mean lifetime (ML) for the five "active" states of the Active (closed circles and boxes) and Sham (open circles and boxes) groups. Cognitive load reduced the FO and ML of the Task Negative ("Task –") state and the FO of the Task Positive ("Task +") state. Importantly, α-tACS reduced the FO and ML of the Task Negative state, regardless of load levels. Furthermore, interaction effects of Group and Load on FO and

ML of the Distraction state indicate that α-tACS downregulated this state in the high load. Center red lines represent the mean values, with the grey box and the encompassing box representing the mean +/- 1.96 SEM and the mean +/- 1 SD, respectively. * $p < 0.05$; ** $p < 0.01$; † $p < 0.1$.